# INTERFERENCE-RESISTANT DETECTION BASED ON TIME-FREQUENCY SUBSPACES

*Jean-Paul G. Gallaire and Akbar M. Sayeed*
Department of Electrical and Computer Engineering
University of Wisconsin–Madison
Madison, WI 53706
akbar@engr.wisc.edu gallaire@ese-metz.fr

## ABSTRACT

The difficulty of modeling interference is one of the main problems in constructing an efficient interference-resistant detector. We present a new detector which exploits the signal correlation structure to account for interference. In order to make a decision between two composite hypotheses, our detector uses the generalized likelihood ratio test. Preliminary results suggest that the resulting detection scheme achieves high performance in presence of strong interference.

## 1. INTRODUCTION

The problem of detecting non-stationary stochastic signals in the presence of interference occurs in many important applications, including mobile wireless communications and radar/sonar processing. Inferring the structure of interference and incorporating it efficiently in detector design is a key issue in such applications.

We present a new data-driven framework for attacking this important problem. One of the key challenges in data-driven methods is to isolate signal and interference structure/features from available data. Even if labeled training data is available, reliable detector design necessitates the exploitation of some inherent structure due to the limited amount of data typically available. Our approach is based on second-order statistics and exploits *a priori* knowledge about the signal correlation structure to *implicitly* account for interference.

Time-frequency and wavelet bases often provide a natural framework for modeling the signal correlation structure. For example, in wireless communications and active sonar processing, the channel induces a canonical basis, comprised of time-frequency shifted copies of the transmitted waveform, for low-dimensional modeling of the signal correlation function [1].

In the next section, we present a general result on interference-resistant detector design that exploits signal structure. Section 3 describes a canonical signal model that is applicable in broadband signaling over dispersive channels, such as in radar/sonar processing and wireless communications. Section 4 exploits the signal model of Section 3 to formulate a framework for interference-resistant detector design in composite hypothesis testing scenarios that are particularly relevant in radar/sonar processing. We present some simulation results in Section 5, followed by conclusions in Section 6.

## 2. CONSTRAINED SUBSPACE DETECTOR DESIGN

Consider the binary hypothesis testing problem

$$\begin{aligned} H_0 &: \mathbf{x} = \mathbf{w}+\mathbf{n} \\ H_1 &: \mathbf{x} = \mathbf{s}+\mathbf{w}+\mathbf{n} \end{aligned} \tag{1}$$

where $\mathbf{x} \in \mathbb{C}^N$ is an $N$-dimensional complex-valued observation vector, $\mathbf{s}$ denotes the non-stationary stochastic signal of interest, $\mathbf{w}$ denotes the non-stationary stochastic interference, and $\mathbf{n}$ denotes zero-mean additive complex white Gaussian noise with variance $\sigma^2$. Our second-order framework is motivated by the detector structure in the Gaussian case when both $\mathbf{s}$ and $\mathbf{w}$ are zero-mean Gaussian signals with correlation matrices $\mathbf{R}_s$ and $\mathbf{R}_w$, respectively. It is instructive to consider two detectors which strike two extreme performance-versus-complexity tradeoffs.

The optimal detector for (1) in the Gaussian case is given by the quadratic test statistic [2]

$$L_o(\mathbf{x}) = \mathbf{x}^H(\mathbf{R}_0^{-1} - \mathbf{R}_1^{-1})\mathbf{x}, \tag{2}$$

where $\mathbf{R}_1 = \mathbf{R}_s + \mathbf{R}_w + \sigma^2\mathbf{I}$ and $\mathbf{R}_0 = \mathbf{R}_w + \sigma^2\mathbf{I}$. If labeled ($H_0$ versus $H_1$) training data is available, $\mathbf{R}_1$ and $\mathbf{R}_0$ can be estimated, in principle, to design the detector. However, due to the nonlinear dependence of $L_o(\mathbf{x})$ on $\mathbf{R}_1$ and $\mathbf{R}_0$, the resulting detector is susceptible to estimation errors particularly in the case of limited training data. Moreover, the structure of $L_o(\mathbf{x})$ becomes particularly complicated if the signal of interest $\mathbf{s}$ exhibits some unknown parameters, such as delay, that have to be taken into account [3, 4]. On the other hand, in the absence of interference ($\mathbf{w} = \mathbf{0}$), a fairly robust design is provided by the locally optimal processor

$$L_{lo}(\mathbf{x}) = \mathbf{x}^H\mathbf{R}_s\mathbf{x}, \tag{3}$$

which is based on a low signal-to-noise ratio assumption [3, 2]. Even though (3) is less sensitive to estimation errors in data-driven design, it is only acceptable in the absence of strong interference.

Both the above detectors are nonnegative definite quadratic forms and represent two extremes. The detector (2) is optimal, but has a complicated structure. On the other hand, the locally optimal detector (3) is simple but is susceptible to interference. Our design formulation strikes a balance between the two extremes: it designs a nonnegative definite detector by enhancing the simple detector $L_{lo}(\mathbf{x})$ in (3) via interference suppression. Our detector design is based on the following constrained optimization problem

$$\begin{aligned} \mathbf{Q}_c &= \arg\min_{\mathbf{Q}\geq\mathbf{0}} \mathrm{E}[\mathbf{x}^H\mathbf{Q}\mathbf{x}] = \arg\min_{\mathbf{Q}\geq\mathbf{0}} \mathrm{tr}(\mathbf{Q}\mathbf{R}) \\ \text{s.t.} \quad & \mathrm{E}[\mathbf{s}^H\mathbf{Q}\mathbf{s}] = \mathrm{tr}(\mathbf{Q}\mathbf{R}_s) = 1, \end{aligned} \tag{4}$$

where $\mathbf{R} = \mathrm{E}[\mathbf{x}\mathbf{x}^H]$ denotes the data correlation matrix, which could be either $\mathbf{R}_0$ or $\mathbf{R}_1$, and $\mathrm{tr}(\cdot)$ denotes the trace of a matrix. The resulting detector is given by

$$L_c(\mathbf{x}) = \mathbf{x}^H\mathbf{Q}_c\mathbf{x}. \tag{5}$$

The intuition behind the above formulation is that the optimal detector $\mathbf{Q}_c$ passes the components of $\mathbf{x}$ in the "direction" of $\mathbf{s}$ at a fixed gain via the constraint, while suppressing the interference due to the minimization of output

power of the detector. Our interference-resistant detection framework is based on the following solution to the above optimization problem, which we state without proof.

**Theorem.** The solution to (4) is given by

$$\mathbf{Q}_c = \sum_{k=1}^{K} \alpha_k \mathbf{u}_k \mathbf{u}_k^H, \tag{6}$$

where the $\mathbf{u}_k$'s are the $K \geq 1$ generalized eigenvectors corresponding to the largest generalized eigenvalue $\lambda_{max}$ of

$$\mathbf{R}_s \mathbf{u} = \lambda \mathbf{R} \mathbf{u}, \tag{7}$$

and the $\alpha_k \geq 0$ are chosen to satisfy the constraint in (4). □

The detector $L_c$ has the interesting property that its expected output power can be expressed as

$$\mathrm{E}[L_c(\mathbf{x})] = \mathrm{E}[\mathbf{x}^H \mathbf{Q}_c \mathbf{x}] = \mathrm{tr}(\mathbf{Q}_c \mathbf{R}) = \frac{1}{\lambda_{max}}. \tag{8}$$

The above property suggests the following general detection procedure: for each observation interval, solve the generalized eigenvalue problem (7), and the resulting value of the maximum eigenvalue $\lambda_{max}$ serves as the test statistic to distinguish between the two hypotheses.

The novelty of the above result is that it implicitly accounts for the interference by exploiting the signal correlation structure $\mathbf{R}_s$ via (4). In practice, $\mathbf{R}$ can be estimated from data, whereas $\mathbf{R}_s$ can be modeled analytically via *a priori* knowledge. Furthermore, appropriate modeling of $\mathbf{R}_s$ can result in simple detector designs. In particular, the focus of this paper is on a canonical representation of $\mathbf{R}_s$ for time- and frequency-dispersive channel which leads to a simple and efficient solution of the generalized eigenvalue problem.

## 3. CANONICAL SIGNAL REPRESENTATION

Time-frequency or wavelet subspaces provide a natural and powerful approach for modeling the structure of $\mathbf{R}_s$. The focus of this paper is on the detection of broadband signals over time- and frequency-dispersive channels. Such problems arise in many applications, including spread-spectrum wireless communications, and radar/sonar processing. The effect of a time-frequency dispersive channel can be generally expressed as [5]

$$s(t) = \int_0^{T_{max}} \int_{-F_{max}}^{F_{max}} H(\theta, \tau) q(t-\tau) e^{j2\pi\theta t} d\theta d\tau \tag{9}$$

where $q(t)$ is the transmitted waveform, $H(\theta, \tau)$ is the channel *spreading function*, and $T_{max}$ denotes the *delay (time) spread* and $F_{max}$ the *Doppler (frequency) spread* of the channel. The waveform $q(t)$ is typically broadband, such as a spread-spectrum symbol waveform in wireless communications [6, 1] or a linear FM pulse in radar/sonar [7].

Due to the finite time-bandwidth-product (TBP) of $q(t)$, (9) admits the following canonical low-dimensional characterization [1, 8]

$$s(t) \approx \sum_{l=0}^{L} \sum_{p=-P}^{P} \widehat{H}\left(\frac{p}{T}, \frac{l}{B}\right) q\left(t - \frac{l}{B}\right) e^{j\frac{2\pi p t}{T}} \tag{10}$$

where $T$ is the duration and $B$ the bandwidth of $q(t)$, and $\widehat{H}(\theta, \tau)$ is a time-frequency smoothed version of $H(\theta, \tau)$ [1]. $L$ and $P$ denote the number of distinct time delays and Doppler shifts determined by the temporal signaling resolution $1/B$ and spectral resolution $1/T$: $L = \lceil T_{max} B \rceil$ and $P = \lceil F_{max} T \rceil$ [1]. A very important feature of the canonical representation (10) is that the time-frequency shifted waveforms

$$q_{p,l}(t) = q(t - l/B) e^{j2\pi p t/T} \tag{11}$$

form an approximately orthogonal basis for representing the channel distorted signal. Furthermore, for the wide-sense stationary uncorrelated scatterer (WSSUS) channel model [5], the sampled channel coefficients $H_{p,l} = \widehat{H}(p/T, l/B)$ are approximately uncorrelated [1]. Thus, (10) is like a Karhunen-Loeve representation of $s(t)$ with a corresponding approximate eigenrepresentation given by

$$R_s(t_1, t_2) \approx \sum_{l=0}^{L} \sum_{p=-P}^{P} \Psi_{l,p} q\left(t_1 - \frac{l}{B}\right) q^*\left(t_2 - \frac{l}{B}\right) e^{j\frac{2\pi p(t_1 - t_2)}{T}} \tag{12}$$

Note that (12) is a "diagonal" representation in terms of the approximately orthogonal basis waveforms $q_{p,l}(t)$.

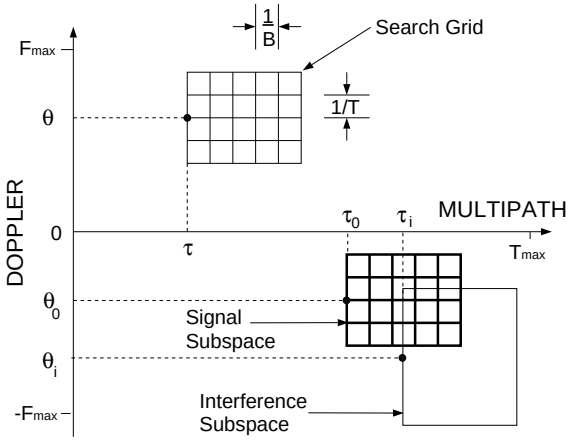


**Figure 1. Basic detector operation in $\mathcal{D}$.**

## 4. DETECTOR DESIGN IN CANONICAL SIGNAL REPRESENTATION

Recall that detector design in Section 2 exploits *a priori* information about $\mathbf{R}_s$. In this section, we combine the canonical $\mathbf{R}_s$ structure in (12) with the framework of Section 2 to design interference resistant detectors applicable in radar/sonar scenarios. We consider a *composite hypothesis testing* problem which is appropriate in radar/sonar applications [3, 2]:

$$\begin{aligned} H_0 &: \mathbf{x} = \mathbf{w} + \mathbf{n} \\ H_1 &: \mathbf{x} = \mathbf{s}^{(\theta_0, \tau_0)} + \mathbf{w} + \mathbf{n} \end{aligned} \tag{13}$$

where $\tau_0$ and $\theta_0$ are the *unknown* nominal delay and Doppler of the signal of interest $\mathbf{s}(\theta_0, \tau_0)$ which corresponds to a sampled version of $s^{(\theta_0,\tau_0)}(t) = s(t-\tau_0)e^{j2\pi\theta_0 t}$ as in (10). We assume knowledge of the transmitted broadband pulse $q(t)$, the duration $T$ and bandwidth $B$, and the number of delay and Doppler components $L$ and $P$ in (10). Furthermore, the scattering statistics $\Psi_{p,l}$ corresponding to $s(t)$ are also known (which do not depend on $(\theta_0, \tau_0)$. No information about noise and interference is assumed known.

To deal with the unknown parameters $(\theta_0, \tau_0)$, we propose the following detector structure which is motivated by the

generalized likelihood ratio test [2, 3]

$$L(\mathbf{x}) = \max_{(\theta,\tau)\in\mathcal{D}} L_c^{(\theta,\tau)}(\mathbf{x}) = \max_{(\theta,\tau)\in\mathcal{D}} \frac{1}{\lambda_{max}^{(\theta,\tau)}}, \qquad (14)$$

where $L_c^{(\theta,\tau)}(\mathbf{x})$ constitutes the constrained detector (5) corresponding to $s^{(\theta,\tau)}(t)$ (and $\mathbf{R}_s^{(\theta,\tau)}$), and $\mathcal{D}$ denotes a delay-Doppler region containing the possible unknown values of $(\theta_0, \tau_0)$.

For each fixed $(\theta, \tau)$, the structure of $L_c^{(\theta,\tau)}(\mathbf{x})$ is derived by incorporating the $\mathbf{R}_s^{(\theta,\tau)}$ model given by (12) in the detector design dictated by the Theorem. It follow from (12) that $\mathbf{R}_s^{(\theta,\tau)}$ admits the following approximate eigendecomposition:

$$\mathbf{R}_s^{(\theta,\tau)} \approx \mathbf{V}^{(\theta,\tau)} \mathbf{\Lambda}_s \mathbf{V}^{(\theta,\tau)H} \qquad (15)$$

where $\mathbf{V}^{(\theta,\tau)}$ is an (approximately) orthogonal matrix corresponding to the $(L+1)(2P+1)$ basis functions (11), all time-frequency shifted by $(\theta, \tau)$, and $\mathbf{\Lambda}_s$ is a diagonal matrix corresponding to the powers $\Psi_{p,l}$ in the different time-frequency eigencoordinates. Furthermore, since the interference $w(t)$ can also be modeled as the transmitted pulse $q(t)$ passing through a time-frequency dispersive channel,[1] with different parameters than those corresponding to $s^{(\theta,\tau)}(t)$, the matrix $\mathbf{V}^{(\theta,\tau)}$ also approximately diagonalizes $w(t)$ and $n(t)$. Thus, the generalized eigenequation (7) can be expressed as

$$\mathbf{\Lambda}_s \mathbf{v}^{(\theta,\tau)} = \lambda \mathbf{\Lambda}^{(\theta,\tau)} \mathbf{v}^{(\theta,\tau)} \qquad (16)$$

where $\mathbf{\Lambda}^{(\theta,\tau)} = \mathbf{V}^{(\theta,\tau)H} \mathbf{R} \mathbf{V}^{(\theta,\tau)}$ is the representation of the data correlation matrix and $\mathbf{v}^{(\theta,\tau)}$ is a corresponding representation of the generalized eigevectors in the $(L+1)(2P+1)$ eigencoordinates corresponding to $\mathbf{R}_s^{(\theta,\tau)}$. The characterization of the maximum generalized eigenvalue of (16) is very simple in those coordinates:

$$\lambda_{max}^{(\theta,\tau)} = \max_{1\le i\le (L+1)(2P+1)} (\mathbf{\Lambda}^{(\theta,\tau)-1} \mathbf{\Lambda}_s)_{i,i}. \qquad (17)$$

The final detector (14) thus takes the form

$$L(\mathbf{x}) = \max_{(\theta,\tau)\in\mathcal{D}} \left( \min_{1\le i\le (L+1)(2P+1)} (\mathbf{\Lambda}_s^{-1} \mathbf{\Lambda}^{(\theta,\tau)})_{i,i} \right). \qquad (18)$$

We note that the above detector operates in the transformed coordinates $\mathbf{z}^{(\theta,\tau)} = \mathbf{V}^{(\theta,\tau)}\mathbf{x}$ for $(\theta, \tau) \in \mathcal{D}$, which can be efficiently computed via a sampled short-time Fourier transform (STFT) as evident from the definition of the underlying basis functions (11). The diagonal matrix $\mathbf{\Lambda}^{(\theta,\tau)}$ represents the expected received power in the transformed coordinates. $\mathbf{\Lambda}^{(\theta,\tau)}$ in (18) can be estimated by averaging the STFT coefficients over multiple received pulse waveforms, and $\mathbf{\Lambda}_s$ is based on our *a priori* knowledge of signal power in the eigencoordinates. A decision is made by comparing the test statistic $L(\mathbf{x})$ to a threshold $\gamma$: if $L(\mathbf{x}) > \gamma$, $H_1$ is true, otherwise $H_0$ is true. A schematic depicting the basic detector operation in (18) is shown in Figure 1. The search grid corresponds to the data correlation matrix $\mathbf{\Lambda}^{(\theta,\tau)}$ at the current search location $(\theta, \tau)$. It is moved at each possible location of $\mathcal{D}$ in order to compute $\lambda_{max}^{(\theta,\tau)}$ as in (17). The final detector output used to make the decision between the two hypotheses is then computed from the $\lambda_{max}^{(\theta,\tau)}, (\theta, \tau) \in \mathcal{D}$, as in (14).

The threshold $\gamma$ used to perform the decision is set using the probability of false alarm (PFA) which depends on the signal to interference and noise ratio (SINR) at every time-frequency coordinate. Good bounds for $\gamma$ can be obtained assuming a uniform power distribution for interference. However, due to lack of space,a detailed analysis of the threshold is beyond the scope of this paper.

It is worth noting the $(\theta, \tau)$ location at which the maximum occurs in (18) also provides an estimate of the nominal delay-Doppler coordinates of $s^{(\theta_0,\tau_0)}(t)$, which provide crucial information about the distance and velocity of the target representing the signal of interest.

## 5. RESULTS

For the experiments, we generate the data on a sub-sampled version of the $(\theta, \tau)$ grid sampled at the critical sampling rates given by (B,T) in (10). This allows us to model the nominal delay-Doppler coordinates for the signal and the interference as "continuous" random variables which do not depend on the critical sampling. The signal of interest and the interference are generated as linear combinations of time-frequency shifted versions of the transmitted waveform as in (10). In the case of the signal, the coefficients of each time-frequency component are computed according to the channel statistics $\Psi_{l,p}$. The signal and the interference are then shifted in time and frequency so that their nominal delay-Doppler coordinates are $(\theta_0, \tau_0)$ and $(\theta_i, \tau_i)$ respectively, as seen in Figure 1. Finally white Gaussian noise is added.

With such a generation scheme, the performance of our detector in several different cases of overlap between signal and interference, and for different signal to interference and noise ratios (SINR) can be explored.

Figures 2 and 3 show the Receiver Operating Characteristics (ROC) curves of our detector for two different SINR and the same partial overlap. As expected, the performance of the detector gets better for higher SINR. However, as seen from Figure 3, our detector can still achieve good performance in very bad situations as long as enough realizations of observations are available to estimate the statistics of the data. In fact, in most cases, it is even possible to achieve perfect detection.

Figure 4 shows the performance of the detector for different cases of overlap at the same SINR. It is interesting to see that more overlap does not necessary decrease the detector accuracy. In fact, we observe the opposite behavior: less overlap between the signal and the interference results in lower performance of the detector. This effect is due to the composite hypothesis testing. The detector must not only decide whether the signal of interest is present, it also has to estimate the localization of this signal. In the case of complete overlap, the detector cannot hesitate between two different locations. On the other hand, when there is no overlap, the detector needs more observations to decide between the location of the signal of interest and the location of the interference.

However, in all different cases of overlap, our detector can still differentiate between signal of interest and interference. From the Figure 5, we can see that this does not stand for the locally optimal detector presented in (3). In the case of partial overlap, it seems able to detect the true signal, but in the case when there is no overlap between the true signal and interference, its performance gets worse as the number of realizations increases. In fact, in the second case, the locally optimal detector mistakes the interference for the true signal.

[1] We restrict our attention to interference due to reverberation. The framework can be extended to other forms of interference as well.

## 6. CONCLUSION

We have presented a new detector which proved to be very efficient in the presence of strong interference. Based on the generalized likelihood ratio test, our detector exploits *a priori* knowledge about the signal correlation structure to *implicitly* account for interference. To make the decision between the two hypotheses, the detector output is compared to a threshold. However, due to lack of space, the thresholding analysis was not presented in this paper. This issue will be addressed in a future publication. We will also explore the possibility of using wavelet bases which, thanks to their decorrelation and energy compaction properties, also seem attractive candidates for parsimoniously representing signal correlation structure in applications such as wide-band radar.

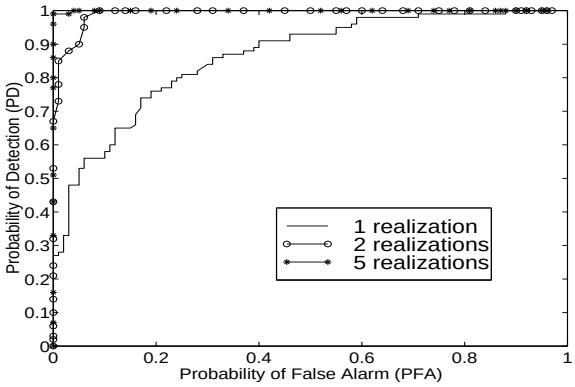


**Figure 2. ROC curves for partial overlap, SINR = 4.36 dB and several realizations of observation**

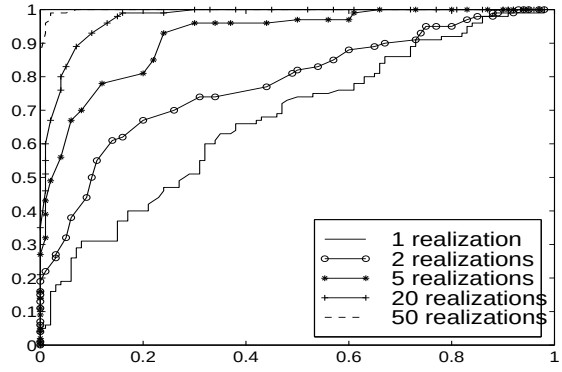


**Figure 3. ROC curves for partial overlap, SINR = -1.34 dB and several realizations of observation**

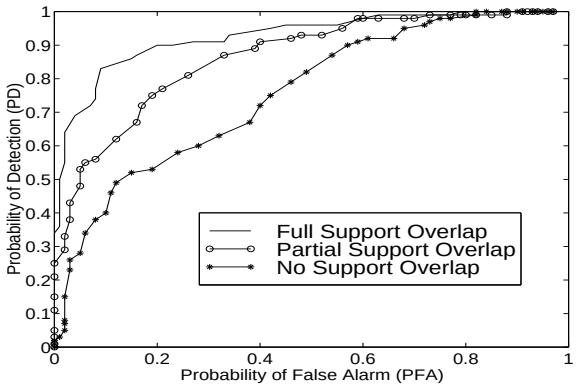


**Figure 4. ROC curves for 3 overlap cases, SINR = 4.36 dB and 1 realization of observation**

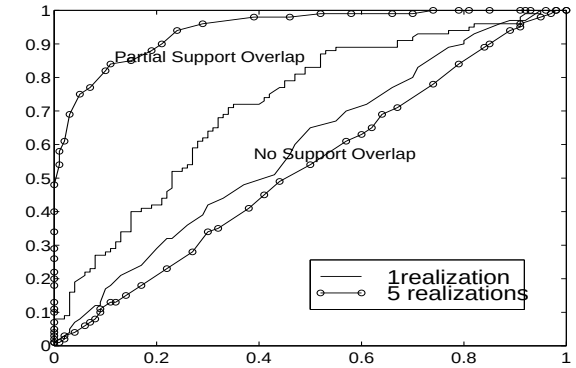


**Figure 5. ROC curves for the locally optimal detector (3) in 2 overlap cases and SINR = 4.36 dB**

## REFERENCES


[1] A. M. Sayeed and B. Aazhang, "Joint multipath-Doppler diversity in mobile wireless communications," *to appear in the IEEE Trans. Commun.*

[2] H. V. Poor, *An Introduction to Signal Detection and Estimation*. Springer-Verlag, 1988.

[3] A. M. Sayeed and D. L. Jones, "Optimal detection using bilinear time-frequency and time-scale representations," *IEEE Trans. Signal Processing*, vol. 43, pp. 2872–2883, Dec. 1995. See also the corrections in vol. 45, pp. 761–762, Mar. 1997.

[4] A. M. Sayeed and B. Aazhang, "Multiuser timing acquisition over multipath fading channels," in *Proc. 1998 Conf. Inf. Sci. Syst. (CISS'98)*, 1998.

[5] P. A. Bello, "Characterization of randomly time-variant linear channels," *IEEE Trans. Commun. Syst.*, vol. CS-11, pp. 360–393, 1963.

[6] J. G. Proakis, *Digitial Communications*. New York: McGraw Hill, 3rd ed., 1995.

[7] H. R. Raemer, *Radar System Principles*. CRC Press, 1997.

[8] A. M. Sayeed and B. Aazhang, "Communication over multipath fading channels: A time-frequency perspective," in *Wireless Communications: TDMA versus CDMA* (S. G. Glisic and P. A. Lippänen, eds.), pp. 73–98, Kluwer Academic Publishers, 1997.